Research in Astronomy and Astrophysics, 22:035015 (14pp), 2022 March https://doi.org/10.1088/1674-4527/ac47ac

Temperature Analysis of Flaring (AR 11283) and Non-flaring (AR 12194) Coronal Loops

Narges Fathalian[1], Seyedeh Somayeh Hosseini Rad[2], Nasibeh Alipour[2], and Hossein Safari[2]
[1] Department of Physics, Payame Noor University (PNU), P.O. Box 19395-3697, Tehran, Iran; narges.fathalian@gmail.com
[2] Department of Physics, Faculty of Science, University of Zanjan, P.O. Box 45195-313, Zanjan, Iran
Received 2021 August 17; revised 2021 December 11; accepted 2021 December 30; published 2022 February 22

Abstract

Here, we study the temperature structure of flaring and non-flaring coronal loops, using extracted loops from images taken in six extreme ultraviolet channels recorded by Atmospheric Imaging Assembly/Solar Dynamics Observatory. We use data for loops of an X2.1-class-flaring active region (AR 11283) during 22:10 UT until 23:00 UT, on 2011 September 6; and a non-flaring active region (AR 12194) during 08:00:00 UT until 09:00:00 UT on 2014 October 26. By using the spatially synthesized Gaussian differential emission measure (DEM) forward-fitting method, we calculate the peak temperatures for each strip of the loops. We apply the Lomb–Scargle method to compute the oscillation periods for the temperature series of each strip. The periods of the temperature oscillations for the flaring loops ranged from 7 to 28.4 minutes. These temperature oscillations show very close behavior to the slow-mode oscillation. We observe that the temperature oscillations in the flaring loops started at least around 10 minutes before the transverse oscillations and continue for a long time duration even after the transverse oscillations ended. The temperature amplitudes increased during the flaring time (20 minutes) in the flaring loops. The periods of the temperatures obtained for the non-flaring loops ranged from 8.5 to 30 minutes, but their significances are less (below 0.5) in comparison with the flaring ones (near to one). Hence the detected temperature periods for the non-flaring loops' strips are less probable in comparison with the flaring ones, and maybe they are just fluctuations. Based on our confined observations, it seems that the flaring loops' periods show more diversity and their temperatures have wider ranges of variation than the non-flaring ones. More accurate commentary in this respect requires more extensive statistical research and broader observations.

Key words: Sun: flares – Sun: corona – Sun: oscillations – stars: imaging – stars: solar-type

1. Introduction

Analyzing the thermal structure of coronal loops is of considerable interest, especially as these magnetic loops have an essential role in heating the solar chromosphere and corona. Such analysis can help to describe how the process of solar flaring is correlated with the loop's thermal structure.

Detections of coronal waves have a historical preview and have been reported several times (e.g., Aschwanden et al. 1999; Berghmans & Clette 1999; Nakariakov et al. 1999; De Moortel et al. 2000; Wang et al. 2003; Verwichte et al. 2004; Wang & Solanki 2004; De Moortel & Brady 2007; Ballai et al. 2011). Coronal seismology and MHD waves have been reviewed widely by De Moortel (2005), Nakariakov & Verwichte (2005), Aschwanden (2006), Banerjee et al. (2007) and De Moortel & Nakariakov (2012). Along with the development of the observations, transverse and longitudinal oscillations have also been studied theoretically (e.g., Gruszecki et al. 2006; Pascoe et al. 2007; Fathalian & Safari 2010; Fathalian et al. 2010; Luna et al. 2010). Coronal seismology techniques help to elicit the information from observations of oscillatory phenomena and the results can be interpreted by using theoretical models (see for e.g., Roberts et al. 1984; Goossens et al. 1992). Oscillatory patterns and processes which happen during solar flares have been interesting and the subject of investigations from different approaches (e.g., Nakariakov et al. 2010; Anfinogentov et al. 2013; Nisticò et al. 2013; Hindman & Jain 2014; Russell et al. 2015). As we know, transverse loop oscillations usually occur in response to a close filament or flare (Wills-Davey & Thompson 1999).

Rapidly decaying long-period oscillations are mostly interpreted as global (or fundamental mode) standing slow magnetoacoustic waves (reviewed by Liu & Ofman 2014, and Wang 2011, also see Ofman & Wang 2002, and for slow-mode observed in fan-loops see Pant et al. 2017). They often occur in hot coronal loops of active regions (ARs), associated with tiny (or micro) flares. Increasing evidence has suggested that the harmonic type of decaying pulsations detected in intensity plots of solar and stellar flares are possibly caused by standing slow-mode waves (see reviews by Van Doorsselaere et al. 2016 and McLaughlin et al. 2018). Excitation, propagation and damping mechanisms of slow-mode waves have been studied theoretically (e.g., Wang et al. 2007, 2015;

Jess et al. 2016; Nakariakov et al. 2017; Nisticò et al. 2017; Kolotkov et al. 2019; Krishna Prasad et al. 2019; Reale et al. 2019; Wang & Ofman 2019). To have a complete overview of slow-mode magnetoacoustic waves in coronal loops see the review by Wang et al. (2021).

Investigating and comparing the thermal structures and oscillations of coronal loops in loops of flaring and non-flaring ARs could help us in better understanding the loops' material oscillations and the flare impact on them. Several different methods have been developed to investigate the thermal structure of the coronal loops and loop strands. The thermal stability of the coronal loops was the subject of research done by Habbal & Rosner (1979) (and references cited therein). McClymont & Craig (1985) stated that a pressure fluctuation must assist asymmetric coronal temperature perturbation. They concluded that coronal loops are fairly stable in the case of uniform heating. Van Doorsselaere et al. (2011) used spectroscopic line ratios to obtain the required temperature (via CHIANTI code) and estimated the adiabatic index of the corona. The dependence of coronal loop temperature on loop length and magnetic field strength is also a favorite topic. For instance, Dahlburg et al. (2018) probed the temperature properties of solar coronal loops over a wide range of lengths and magnetic field strengths via numerical simulations and observed a very high correlation between magnetic field strength and a maximum of the temperature. The effect of temperature inhomogeneity on the periods and the damping times of the standing slow-modes in stratified solar coronal loops was also studied (e.g., Abedini et al. 2012). Fathalian (2019) estimated the loop temperature using the intensity ratios and the Atmospheric Imaging Assembly (AIA) response functions in different wavelengths. Different emission measure computations and methods have been developed to estimate the temperature in the corona, which led to various discussions. Schmelz et al. (2010) analyzed a coronal loop, which was observed on 2010 August 3 by AIA. They took some differential emission measure (DEM) curves, claiming a multithermal rather than an isothermal DEM distribution (for the cross-sectional temperature of the loop). After that, Aschwanden & Boerner (2011) criticized the method of background subtraction which Schmelz et al. had applied. They claimed that the background subtraction method caused their inferred result of a multithermal loop. Aschwanden & Boerner (2011) analyzed a set of a hundred loops and concluded that 66% of the loops could be fitted with a narrowband single-Gaussian DEM model. In this regard, some attention was paid to the instrumental limitations and ability of AIA and Guennou et al. (2012a, 2012b) discussed the accuracy of the DEM diagnostics of solar plasmas with respect to the AIA instrument of Solar Dynamics Observatory (SDO). The abovementioned controversy of whether the cross-field temperatures of coronal loops are multithermal or isothermal continued with Schmelz et al. (2013) (similar to Schmelz et al. 2011). They analyzed twelve loops to investigate their cross-field temperature distributions and revealed the loops' substructure. Based on their achievements, the warmer loops entail broader DEMs. Thereafter, Schmelz et al. (2014) found indications of a relationship between the DEM weighted-temperature and the cross-field DEM width for coronal loops. They argued that cooler loops tend to have narrower DEM widths. This could imply that fewer strands are seen emitting in the later cooling phase, which they claim could potentially resolve the abovementioned controversy. In this subject, Aschwanden et al. (2015) (as well as Aschwanden et al. 2013) developed a method to extract the loop temperature which is based on a Gaussian fit for the DEM, named spatially synthesized Gaussian DEM forward-fitting method.

This paper aims to analyze and compare thermal oscillations of coronal loops in flaring and non-flaring ARs, 11283 and 12194, respectively. The contents of this paper are as follows: In Section 2, we introduce the considered flaring and non-flaring ARs and describe the data employed and the time and properties of the flare which occurred in the AR. In Section 3, we explain the method we use to analyze the time-series of temperatures in different strips of the loops. Section 4 reports our results obtained related to flaring and non-flaring regions. In Section 5, we briefly state a summary of this work.

2. Data

We investigate the thermal structure and treatment of loops in a flaring region to see if it follows the transverse oscillations of the loops, and we examine the thermal fluctuations at the flare time. For this purpose, we select a high energy flare x2.1 for which the transverse oscillations of two loops have been analyzed by Jain et al. (2015). They analyzed intensity variations in the wavelength 171 Å in two coronal loops of this region and detected obvious transverse oscillation with periods of roughly 2 minutes and decay times of 5 minutes for these loops at the flare time. To see the specific thermal properties of the flaring loops, as a blind test, we select a non-flaring AR, extract its loops and analyze their thermal treatment. Then we compare the temperature treatment of the loops at the flaring region with the loops of the non-flaring region to see the differences.

The temperature analysis done here uses extreme ultraviolet (EUV) images from the AIA onboard the SDO. AIA has ten different wavelength channels, three in white light and ultraviolet (UV), and the other seven in EUV channels. Among these seven, the 304 filter, which is mostly sensitive to chromospheric temperatures (in order of $T = 10^{4.7}$ K), not the corona, is not taken into account (Aschwanden et al. 2015). Therefore, we consider the images of the events in the six wavelengths (94, 131, 171, 193, 211, 335 Å). These are covering the coronal temperature range from $T \approx 0.6$ to $T \geqslant 16$ MK.

The two below data sets are finally selected to study thermal variations and coronal loop oscillations in flaring or non-flaring

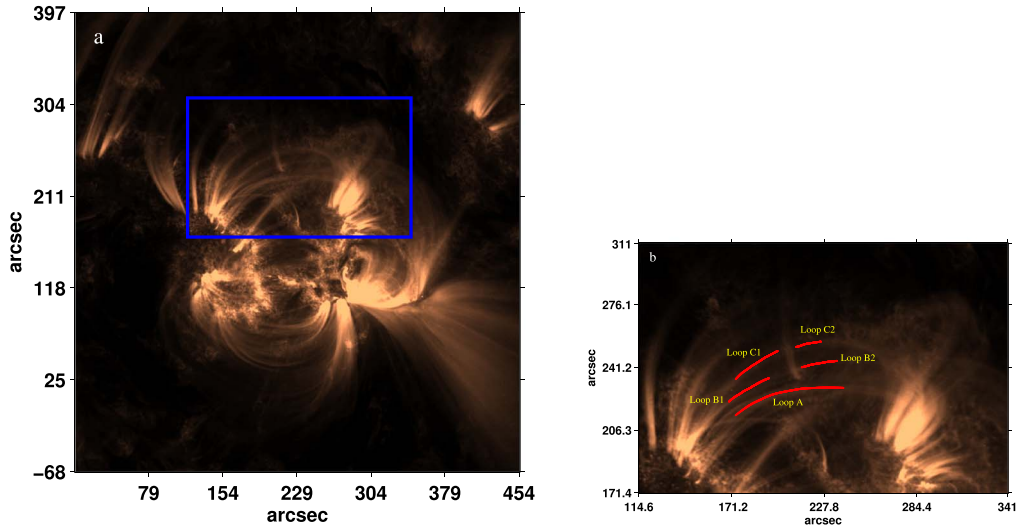

Figure 1. (a) AIA image of the AR 11283 on 2011 September 6, 22:10 UT as seen in the 171 Å filter. (b) Zoom-in view of the area marked by a box is on the left. The selected loops are distinguished in red. The loops A and B are the same loops studied by Jain et al. (2015) (see Figure 3(a) in Jain et al. 2015).

ARs. A few distinct loops are visible in the regions. Finally, these loops are chosen:

1. Three loops of the x-flaring AR 11283: Observationally, X-class flares rarely happen around the loops with the specification we are looking for. So, this selected line-of-sight (LOS) X-flare, which occurs near the loops, is a rare case. We consider EUV images of NOAA AR 11283, in the time period of 22:10 UT until 23:00 UT on 2011 September 6 with the cadence of 12 s. This period of time is selected since no other flare happens then. A few distinct loops are visible and follow-able here during this period. Loop shapes in our AR change permanently; therefore, it is difficult or impossible to follow a loop over a very long time. Hence, it is not useful to extend the time interval of this region to the time before the flare. The transverse oscillations of two loops in this region were analyzed before by Jain et al. (2015). We mark these loops by A and B in Figure 1(b). They detected fundamental mode oscillation with periods of roughly 2 minutes and decay time of 5 minutes for these loops. We are curious to see the loops' thermal oscillations (if any) or thermal fluctuations in this condition. Figure 1(a) (left) displays AR 11283 and the area, indicated by the white box, is featured in a zoom-in view in Figure 1(b) (right) and the five selected parts of the center of the three chosen loops are shown by red lines (a movie of the region is available in this link). As is clear in the movie, these three loops oscillate together and their oscillations decay simultaneously. The center of Figure 1(a) has coordinates at (230, 165) arcsec and its width and height are $450'' \times 456''/\ 750 \times 775$ pixels. The flare occurring in this AR is an X2.1 class flare located close to the disk center at latitude 14° north and longitude 18° west ($269.''9$, $129.''9$). This flare initiates at 22:12 UT, ends about 22:24 UT with the peak at 22:20 UT and is associated with a coronal mass ejection (CME) which occurs from 2011 September 6, 21:36:05T to 2011 September 7, 02:24:05T, with the radial velocity of 469 km s^{-1}, angular width of 252° and position angle of 275° (for more details look at the LASCO CME catalog).[3]
2. Three loops of non-flaring AR 12194: As a blind test, we select three loops of the non-flaring (nonf hereafter) AR 12194 in the smooth time period of 08:00:00 UT until 09:00:00 UT of 2014 October 26. The center of Figure 2(a) has coordinates at (0, −264) arcsec and its width and height are $615'' \times 615''/1025 \times 1025$ pixels. We consider the images of the selected area with the cadence of 12 s in the same six wavelengths mentioned above. These loops are relatively motionless and do not show any transverse oscillation (see the region's movie in the link). We select the loops in such a way that they do not have any crossing over the neighboring loops (from our perspective) during this time. In Figure 2 the selected loops are distinguished in red in the mentioned AR. The size of the final cut of the nonf region (presented on the right) is 351×401 pixels.

The data set is primarily downloaded at level 1 with a pixel resolution of $0.''6$. We use the standard *aia_prep.pro* subroutine available in the SDO package SolarSoftWare (SSW) library to adjust the screen scale between the four arms

[3] Based on data on these websites: https://solarflare.njit.edu/webapp.html and https://www.swpc.noaa.gov/.

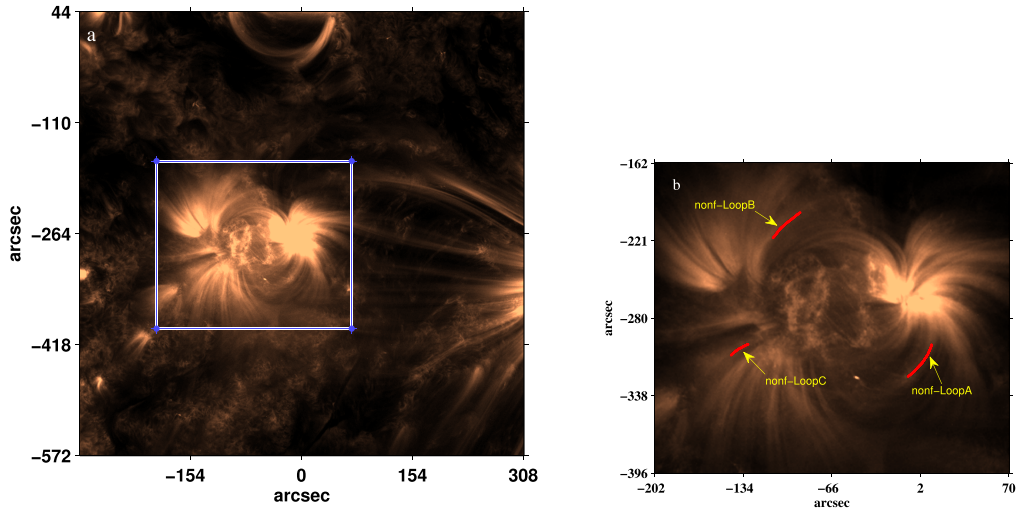

Figure 2. (a) The NOAA AR 12194 on 2014 October 26, at 08:00:00 UT in 171 Å recorded by AIA/SDO. (b) Zoom-in view of the area, marked by a box in the left, the loops are distinguished in red.

of the AIA. This pre-processing step increases the data level from 1 to 1.5, so that finally no jump or sudden movement is observed in the image series. We also utilize the *drot_map. pro* subroutine to correct the differential rotation effect. According to the movie made by pre-processed images, the most obvious loops (marked in the abovementioned figures) are selected in each region (with obvious transverse oscillations in the case of the flaring AR).

3. Temperature Analysis Method

We extract the selected loop segment pixels, for each loop, and calculate the normal vectors to each point of the loop's direction. Then by using these data, we straighten each loop in a considered box with the thickness of 15–40 pixels (macro-pixels, depending on the available empty area around each loop and the distance to the neighboring loop). The area around the loop is needed for calculations of background subtraction. The selected loop segment is cut in all wavelengths and at the same considered box from the set of images. These loop images are necessary prerequisites for our thermal analysis process. Then the loop is divided into different strips and its best division in terms of pixel intervals is considered. To do thermal analysis, we use the spatially synthesized Gaussian DEM forward-fitting method proposed by Aschwanden et al. (2015).

The images in the above six wavelength filters are considered to calculate the temperature in each strip of the loop. The DEM function is considered a single-Gaussian function relative to the temperature determined by the forward fitting method. To obtain the temperature for each loop, we divided the loop into narrow strips, and then the intensity flux was averaged over each strip. The number of each strip is displayed with the index i. One of the usual methods to subtract the background from observed data is fitting a single-Gaussian cospatial function with a linear function on the flux profile. The DEM for each strip is considered to be a single-Gaussian DEM in terms of the logarithm of the temperature, which has three free parameters (Aschwanden & Boerner 2011)

$$\mathrm{DEM}_i = \frac{d\mathrm{EM}_i}{dT} = \mathrm{EM}_{p,i} \exp\left(-\frac{[\log(T) - \log(T_{p,i})}{2\sigma_{T,i}^2} \right). \quad (1)$$

In this expression, $T_{p,i}$ is the DEM peak temperature, $\mathrm{EM}_{p,i}$ is the peak EM function and $\sigma_{T,i}$ is the logarithmic width of the temperature for that strip. To calculate the background-subtracted fluxes (for each strip) we use Equation (6) of Aschwanden & Boerner (2011) (below)

$$F_{0\lambda} = \int \frac{d\mathrm{EM}(T)}{dT} R_\lambda(T) dT = \sum_k \mathrm{EM}(T_k) R_\lambda(T_k). \quad (2)$$

Here, $R_\lambda(T)$ is the instrumental temperature response function of each wavelength filter λ, which is obtained by the code *aia_get_response.pro* in the SSW package. As time has passed, the calibration of the AIA response functions has partly changed. Here, we use the updated calibration of the temperature response functions, for each of the AIA temperature filters, according to the CHIANTI Version 2019 code available in SSW. After forward-fitting the Gaussian DEM to the background-subtracted observed fluxes in multiple wavelengths, the three-fitting parameters, temperature width ($\sigma_{T,i}$), peak of temperature ($T_{p,i}$) and peak emission measure ($\mathrm{EM}_{p,i}$), are found by minimizing χ_i^2.

Our data sample is uneven because of omitting some damaged images in between. Therefore to analyze the temperature oscillations, we use the Lomb–Scargle method. This method implements the periodogram technique, in the

Table 1
The Properties Observed for the Loop Segments of the Flaring AR

F-Loop A (Strip Number)	The Highest Temp.'s Period Observed	Max(log (T))–Min (log(T))	F-Loop B2 (Strip Number)	The Highest Temp.'s Period Observed	Max(log (T))–Min (log(T))
1	9.94	1.09	1	18.07	0.68
2	16.57	0.79	2	24.85	0.83
3	8.46	0.65	3	24.85	0.85
4	28.4	1.11	4	7.36	0.84
5	28.4	0.75	5	8.64	0.85
6	24.85	0.76	6	8.28	0.93
7	22.09	0.58	7	18.07	0.84
8	18.07	1.55	8	28.4	0.73
9	18.07	1.6	F-LoopC1	⋯	⋯
10	12.42	1.57	1	28.4	1.46
11	12.42	1.42	2	22.09	1.34
12	24.85	1.56	3	16.57	1.36
13	19.88	1.6	4	28.04	1.49
14	19.88	1.24	5	24.85	1.6
15	18.07	1.58	6	24.85	1.42
16	19.88	1.45	7	15.29	1.6
17	16.57	0.7	8	13.25	1.56
18	7.36	1.6	9	13.25	1.6
19	8.64	0.95	10	16.57	1.6
20	16.57	1.54	11	16.57	1.6
21	7.36	1.18	12	9.46	1.13
22	7.36	1.51	F-Loop C1	⋯	⋯
23	18.07	1.58	1	18.07	0.88
24	22.09	1.33	2	28.4	0.8
25	24.85	0.72	3	15.29	0.87
F-Loop B1	⋯	⋯	4	16.57	0.93
1	18.07	1.43	5	18.07	1.22
2	15.29	0.76	6	28.4	0.58
3	18.07	0.76			
4	18.07	0.75			
5	18.07	0.59			
6	19.88	0.8			
7	19.88	0.91			
8	19.88	1.36			
9	11.04	1.6			
10	18.07	1.6			
11	18.07	1.6			

Table 2
The Properties Observed for the Loop Segments of the Non Flaring AR

Nonf Loop A (Strip Number)	The Highest Temp.'s Period Observed	Max(log(T))–Min(log(T))
1	24	0.61
2	30	0.95
3	30	0.81
4	20	1.51
5	20	0.77
6	20	0.81
7	11.42	0.71
8	12	0.73
9	30	0.72
10	30	0.77
11	30	0.61
Nonf Loop B (Strip Number)	The highest Temp.'s period observed	Max(log(T))–Min(log(T))
1	26.66	0.36
2	26.66	0.64
3	10.43	0.45
4	12	0.62
5	30	0.98
6	8.57	0.67
Nonf Loop C (Strip Number)	The highest Temp.'s period observed	Max(log(T))–Min(log(T))
1	26.66	0.76
2	26.66	0.75
3	26.66	0.26
4	30	0.27
5	30	0.8

case where the observation times are unevenly spaced (Scargle 1982). The Lomb–Scargle periodogram method is useful in cases where the periodicity of data treatment is not immediately apparent. This method allows efficient computation of a Fourier-like power spectrum estimator from unevenly sampled data, resulting in an intuitive means of determining the period of oscillation (VanderPlas 2018). Therefore we use the Lomb–Scargle Periodogram to efficiently evaluate and estimate the periods of temperature oscillations in our loops. We select the first period related to the highest power frequency, which is obtained by this method. We consider the achieved periods with the highest significances and amplitudes. The most significant (highest) periods observed in temperature (minute) for flaring and nonf loops are listed in Tables 1 and 2, respectively. To estimate the significance of the periods, we computed the probability values (p-values). In the Lomb–Scargle method, the significance returned here is the false alarm probability of the null hypothesis, i.e., as the data are composed of independent Gaussian random variables. Accordingly, low probability values (p-value less than 0.05) indicate a high degree of significance in the associated periodic signal.

4. Results

4.1. Temperature Analysis of Flaring Active Region Loops

Thenceforth, the temperature time-series of different strips of the selected loops are calculated using the method described in Section 3. In the following figures, the vertical axis shows the logarithm of the temperature and the horizontal axis displays the time duration. To be comparable by eyes, all the forthcoming figures (which feature temperature oscillations of the loops) have been co-scaled in the (log) temperature range of 5.7–6.9. The color maps are shown for each temperature map. Loops A, B1, B2, C1 and C2 are subdivided into 25, 11, 8, 12

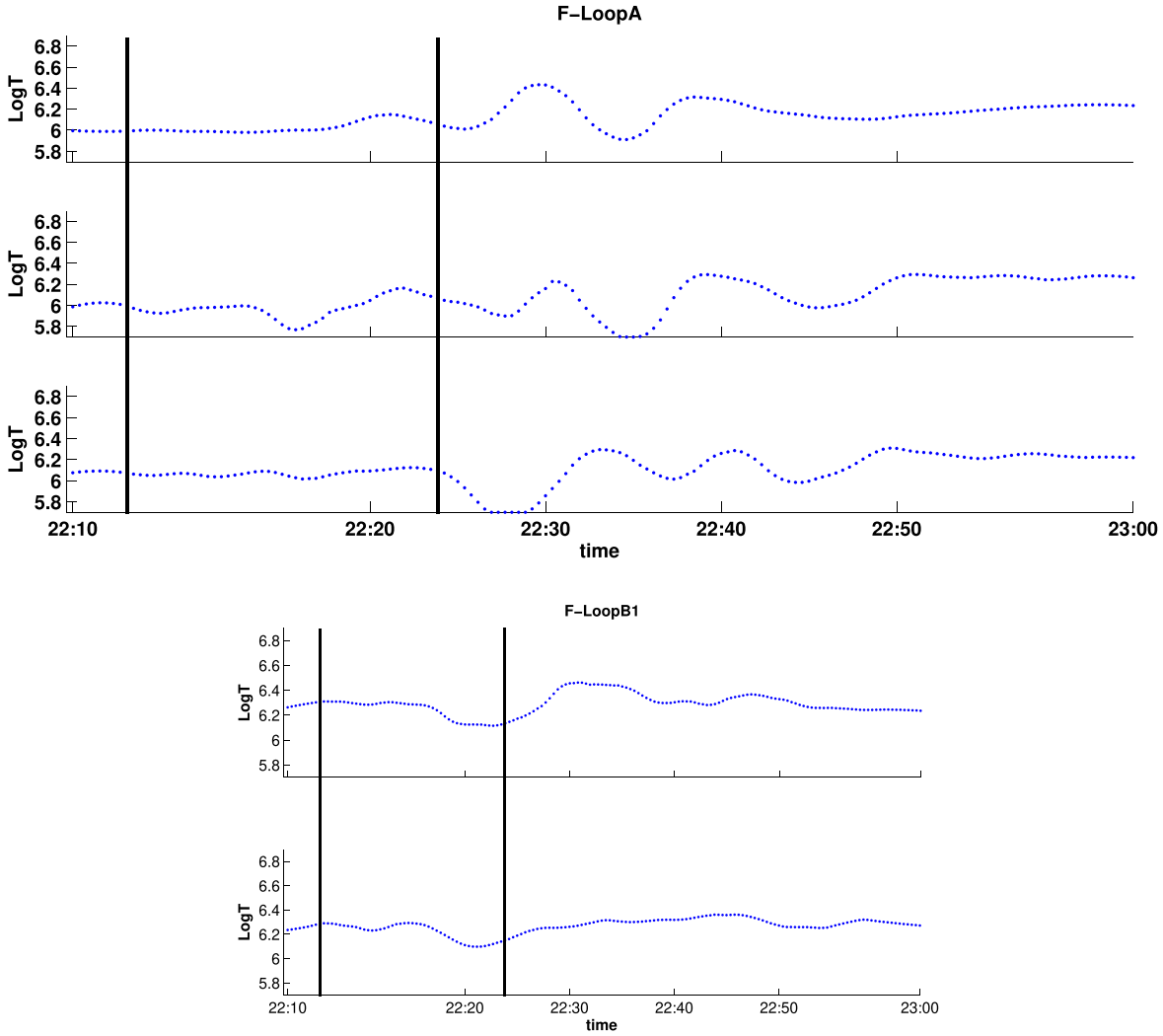

Figure 3. From top to bottom: The time-series of the temperature oscillations for the first three strips of Loop A (strips 1 to 3 from top to bottom, respectively), and the first two strips of Loop B1. The horizontal axis is time and the vertical axis is the logarithm of temperature. The red lines mark the initial and final time of the flare x2.1.

and 6 strips, respectively. Each strip's length is equal to 4 pixels (macro-pixel) for all loops in this paper. For brevity, a few strips' temperature oscillations are presented here. Figure 3 displays the time-series of temperature oscillations for the first three strips of Loop A, and the first two strips of Loop B1. We calculated the errors for each point (temperature) but removed them in the presentation to avoid overcrowding the figures. As we observe in Figures 3 and 4, the temperature oscillations started and increase around 22:12 before the flare peak time (22:20) and are mostly continuing after the flare ended (22:24). These temperature oscillations follow the transverse loop oscillations observed by Jain et al. (2015). As Jain et al. reported, Loops A and B have transverse oscillations with periods of roughly 2 minutes and decay times of 5 minutes, starting at 22:18 around the flare peak time (23:20) and decaying after the flare ended (22:24). So as we observe, the temperature oscillations in these flaring loops happen before the start of their transverse oscillations and are continuing even in the time interval after the transverse oscillations decay, although the temperature oscillations do not decay as rapidly as the transverse oscillations do, and conversely, the loop temperature increases at the end of the oscillating mode (see Figure 4, the temperature map of Loop A, for instance).

We calculate the temperature oscillation periods using the Lomb–Scargle method. We consider the thermal oscillation periods with the highest significances. As this method shows, the most powerful period in the range of data time-series (listed in Table 1) is from 7 to 28.4 minutes observed in the strips of the marked loops of this flaring region. These loops of the flaring region also show some short periods in temperature

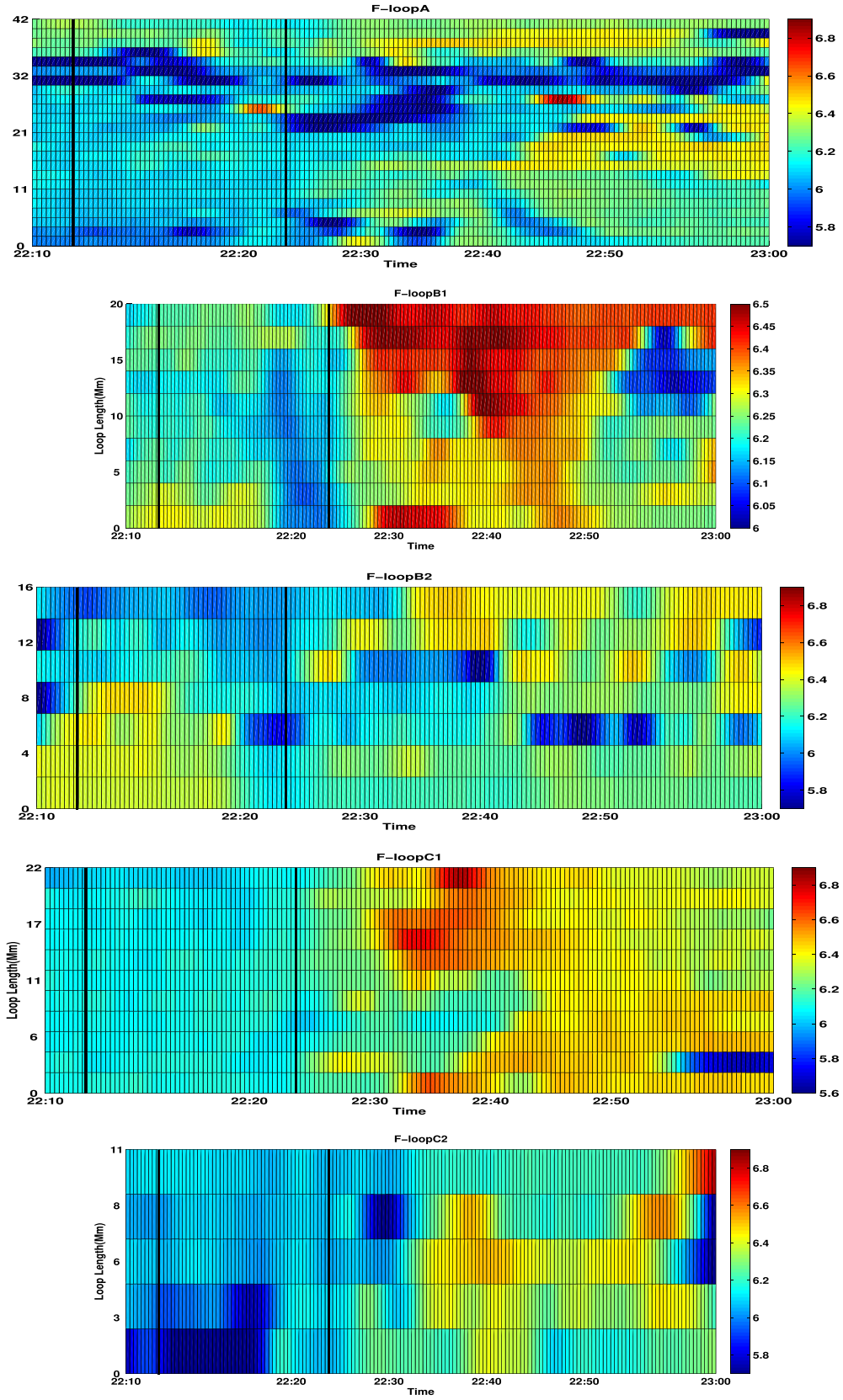

Figure 4. Temperature map of the flaring Loops A, B1, B2, C1 and C2 (from top to bottom respectively) as a time series. The vertical axis is distance along the loop in Mm, and the horizontal axis is time. The colorbar on the left shows the colors considered for the temperature range.

oscillations in which some are less than 10 minutes (as listed in Table 1). These short periods are more frequently observed in the loops of the flaring AR. Such short periods are very scarce for the loops of the nonf AR (compare Tables 1 and 2).

The first column in Table 1 is the number of every strip along the loop. The second column is the period of the most powerful frequency observed for the loop strips, calculated by the Lomb–Scargle method. The third column shows the maximum of log(T) minus its minimum in each strip. The columns of Table 2 are exactly the same as those in Table 1; the only difference is that Table 2 is for the nonf loops.

Loop A has a length of 42.3 (Mm) which is the length of the selected part of the loop marked in Figure 1(b). The mean of the parameter (Max(log$T$)–Min(log$T$)) for the strips of Loop A is 1.21. The mean of the temperature (log) of this loop over time is 6.15 ± 0.25. Loop B1, divided into 11 strips, has a length of 20.24 (Mm). The mean of (Max(log$T$)–Min(log$T$)) and the mean of temperature for this loop are 1.10, and 6.28 ± 0.22 respectively. Loop B2, which has eight strips, with a length of 15.61 (Mm), has a mean temperature (log) of 6.21 ± 0.21. The mean of (Max(log$T$)–Min(log$T$)) is 0.81 through this loop segment. Loops C1 and C2, divided into 12 and 6 strips, have lengths of 22.08 and 11.06 (Mm), mean temperatures of 6.25 ± 0.22 and 6.14 ± 0.25 (log), and means (Max(log$T$)–Min(log$T$)) of 1.48 and 0.88, respectively.

We observe that despite the temperature oscillations, the flaring loops show a temperature rise at the end of the considered time interval (Figure 3). As their temperature maps also affirm, the oscillations follow with a relatively sensible rise in the final temperature of the loop segments (Figure 4), although in the case of transverse oscillations, the loops oscillate as the flare occurs and then the oscillations decay and stop. In the case of temperature oscillations, the temperatures of the various strips of the loops oscillate and, at the end of the flare occurrence, they arrive at a relatively higher value of temperature on average.

Figure 4 depicts the temperature maps of flaring loops A, B1, B2, C1 and C2, from top to bottom respectively, as a time series. In each plot, the vertical axis is the distance along the loop segment in Mm and the horizontal axis represents time. The color bar (on the left) signifies the temperature range. Each separate grid part on the map corresponds to one strip. Figure 4 demonstrates that the temperature for most of the strips increased, bypassing a few oscillations. Before the end of the time duration, some strips become hotter (yellow ones) and some cooler (blue ones). Loop B1 is colder at the early times of the duration and becomes hotter at the middle and end times with a swing to lower temperatures again (see Figure 4). There are some temperature fluctuations at the middle times (the red and green stripes) while at the end the strip temperatures are smoother with less fluctuations. The temperature map of the loop segment B2 (Figure 4) shows that at the beginning of the time duration, the first strips of the loop are hotter, and the last ones are colder, but at the end times this pattern is reversed in this loop segment. In loop segment C1 (Figure 4), the temperature fluctuations are mainly observed to start after the end of the flare (22:24), and at the end time (23:00) the temperature is much higher than the beginning. The temperature is also increasing after the flare time (22:24) for Loop C2 (see Figure 4). This happens with some oscillations in the strips' temperatures. So as Figure 4 demonstrates, the temperature increases with some fluctuation in most of the flaring loops' strips after the flare time. According to these temperature maps, the temperature fluctuations in the flaring loops are increasing at the flaring time and around 20 minutes after that.

We expect the flaring loops to cool down as a result of heat conduction and radiative cooling. Hence this relative temperature increase should be scrutinized. As we investigated, this temperature rise is also followed by an intensity time-series. As the intensity time-series show, the related intensity in Loop A of the flaring AR increases at the end of the time duration. To be assured, the authors also checked the wavelength of Fe XVIII which has a peak formation temperature of 7×10^6 K (Ugarte-Urra & Warren 2014). By applying the method developed by Warren et al. (2012) the contribution of the Fe XVIII emission line can be isolated from AIA 94 Å to analyze the evolution of hot plasma in the loops. We do it to omit contamination from the cooler plasma (mostly around 1 MK) which also contributes to this AIA channel (Boerner et al. 2012). This is done by subtracting the contaminating warm (i.e., around 1 MK) component to the bandpass. This warm contribution is calculated from a weighted combination of the emission from the AIA 171 Å and 193 Å channels dominated by Fe X and Fe XII emission, respectively. This intensity analysis is done directly and it has not gone through any other process like the thermal analysis. For this purpose, we applied the formulation (1) used by Li et al. (2015). Plots in Figure 5 display the intensity map and the mean intensity variation of the wavelength Fe XVIII, for Loop A of the flaring region, in the top and bottom panels respectively. As these plots show, this intensity is also higher at the end of the time duration with respect to the flare time. It seems to us that the expected cooling has not occurred in these flaring loops yet, even after the flare occurrence in the probed duration due to some plausible reasons. We consider that the mentioned simultaneous CME (see Section 2) which this flare is associated with could cause this increase in temperature. We can be sure that the source of this CME is AR 11283 (Romano et al. 2015). This CME is in our flare region, hence the loops receive energy even after the flare occurrence and it is probably the reason why the expected cooling does not occur.

The thermal oscillation periods, obtained with the Lomb–Scargle method, do not have the same significance in all strips of the loops, but for most strips of the flaring loops, the

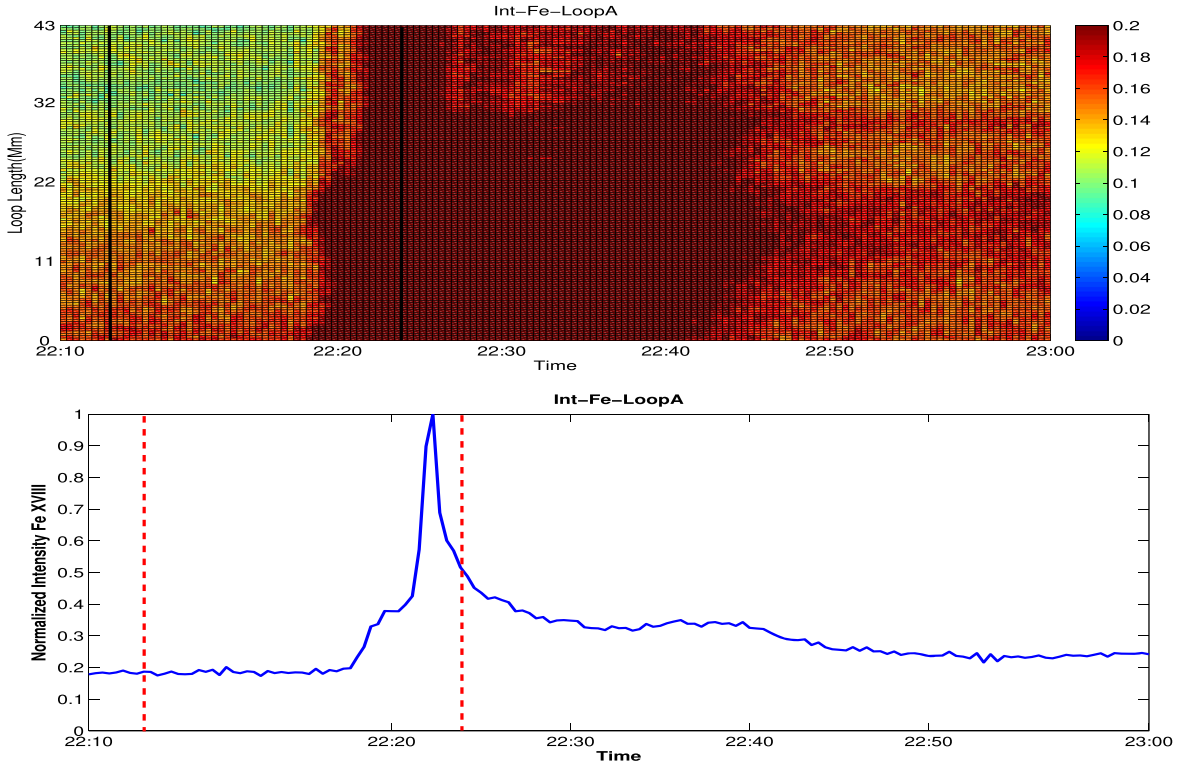

Figure 5. Normalized intensity map of flaring Loop A for the wavelength Fe XVIII, and mean intensity of Fe XVIII (from top to bottom). The vertical axis is the distance along the loop in Mm for the first plot, and normalized intensity is in the second plot. The horizontal axis is time. The colorbar on the left shows the colors considered for the intensity range.

significances are very near to one. To be assured about these oscillations, we examined the intensity time-series for each strip of the loops and we observed that this loop's intensities also manifest intensity oscillations (i.e., alongside the loop). The most probable dominant periods observed in intensity for wavelength of 171 Å is 18.22, and 16.7 minutes for strips of F-Loop A, 16.7, and 18.22 minutes for strips of F-Loop B1, 16.70, and 12.52 for F-Loop B2, and 16.7 for F-Loop C1 and F-Loop C2. These periods are on the same order as the observed thermal oscillation periods. The intensity in this time series has not passed any thermal process but still shows oscillation periods close to thermal ones, so we think these results confirm the observation of thermal oscillations.

4.2. Temperature Analysis of Non-flaring Active Region Loops

The temperature time-series for different strips of the selected loops of the nonf AR 12194 are calculated using the Lomb–Scargle method. In the following plots (Figure 6), the vertical axis represents the logarithm of the temperature and the horizontal axis corresponds to the time duration. Figure 6 displays the time-series of temperature variations for the first two strips of the nonf Loops A and B. These figures are all co-scaled in the range of 5.7–6.9 for the logarithm of temperature (like the flaring loops range). The most powerful periods, observed in most of these nonf loops' strips (listed in Table 2), are from 8.5 to 30 minutes. Comparing the periods of the loops in the flaring region (Table 1) with the nonf ones (Table 2), we see that the temperature periods of the flaring loops have lower values on average and have more diversity than the nonf ones. As Tables 1 and 2 affirm, the mean temperatures of nonf-loops are lower in comparison with the f-loops, a fact we also expected from common sense. The parameter (Max(log$T$)–Min(log$T$)) in nonf-loops' strips is less than that for the flaring loops' strips.

Nonf Loop A, divided into 11 strips, has the length of 19.91 (Mm) which is the length of the selected part of the loop marked in Figure 2(b). The mean of (Max(log$T$)–Min(log$T$)) for the strips of nonf Loop A is 0.81. The mean of temperature (log) of this loop segment over time is 5.93 ± 0.10. Nonf Loop B, divided into six strips, has the length 11.11 (Mm), and the mean temperature (log) and the mean of (Max(log$T$)–Min(log$T$)) for this loop are 5.99 ± 0.13 and 0.62 respectively. Nonf Loop C, which has five strips, with a length of 10.13 (Mm), has the mean temperature (log) of 5.82 ± 0.12 and the mean (Max(log$T$)–Min(log$T$)) of 0.56.

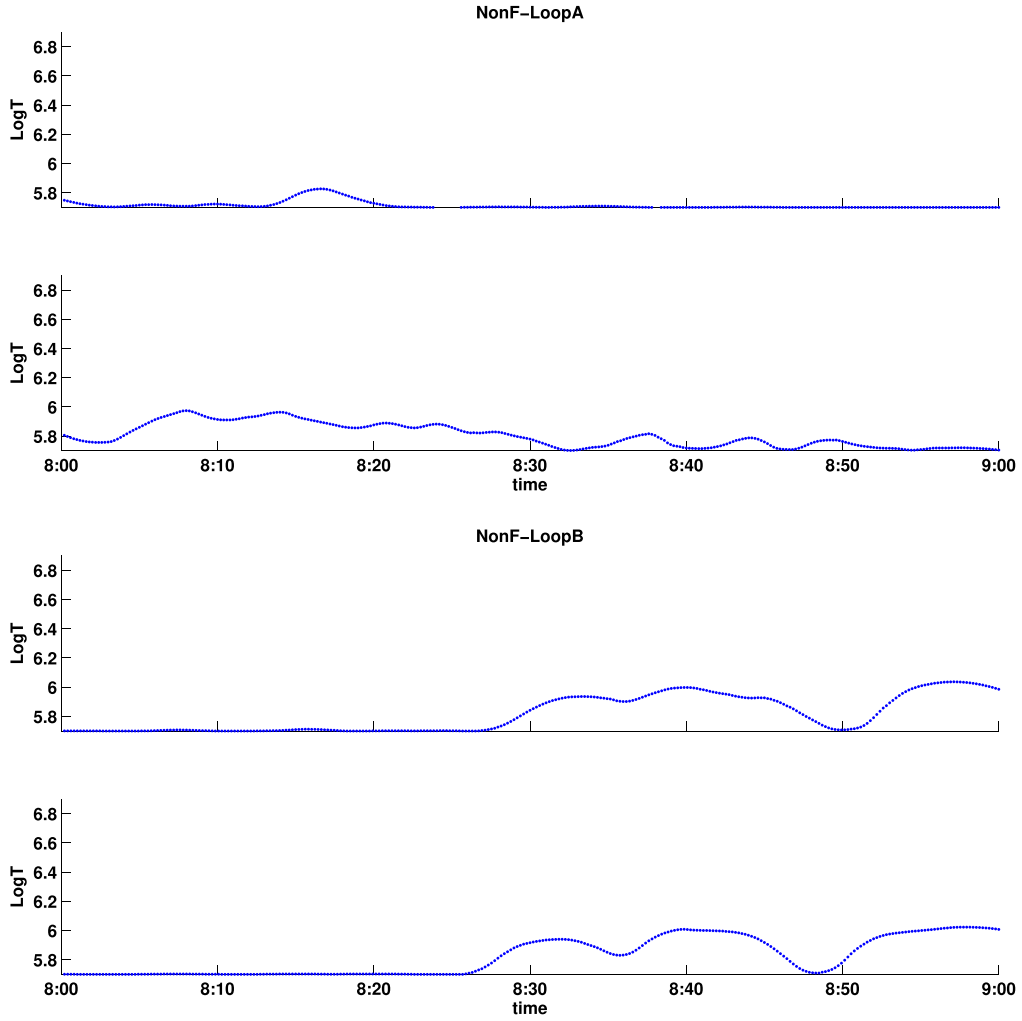

Figure 6. From top to bottom: The time-series of temperature for the first two strips (from top to bottom) of the nonf Loops A and B. Horizontal axis is time and vertical axis is the logarithm of temperature.

The highest period observed for the temperature oscillations of these nonf loops strips is reported in Table 2. As we observe, the temperature periods in these nonf loops are mostly longer than those of the flaring loops (compare the values listed in Tables 1 and 2). Therefore the temperature oscillations of these loops are a little slower than the flaring ones.

Figure 7 features the temperature maps of the nonf Loops A, B and C, from top to bottom respectively, as a time series. In each plot, the vertical axis is the distance along the loop in Mm and the horizontal axis is time. The color bar in the left shows the colors considered for the temperature range. Each separated colored part in the map is one strip. These color maps are all plotted with the same color range for the loops of the flaring region.

As Figure 7 demonstrates, the temperatures of these strips associated with nonf loops are lower and smoother in comparison with the flaring ones (Figure 4). Furthermore, much increase in the temperatures of the strips, which was obvious in the loops of the flaring region toward the end times, is not observed here. The temperatures are also totally lower in the nonf loops in comparison with the flaring loops. Conversely, it seems that different strips of the nonf loops have relatively more similar temperature fluctuations.

As Figure 8 shows, the peaks of the observed temperature periods for the loops' strips of the flaring AR (blue ones) and nonf AR (red ones), are around 18 minutes and 30 minutes, respectively. The temperature periods' diversity is higher in the loops' strips of the flaring AR, and shorter temperature periods (less than 10 minutes, nearer to the transverse oscillations periods) are observed in the case of the flaring loops' strips in comparison with the nonf ones. In addition, Figure 9 shows that the increase and decrease of temperature range, or the

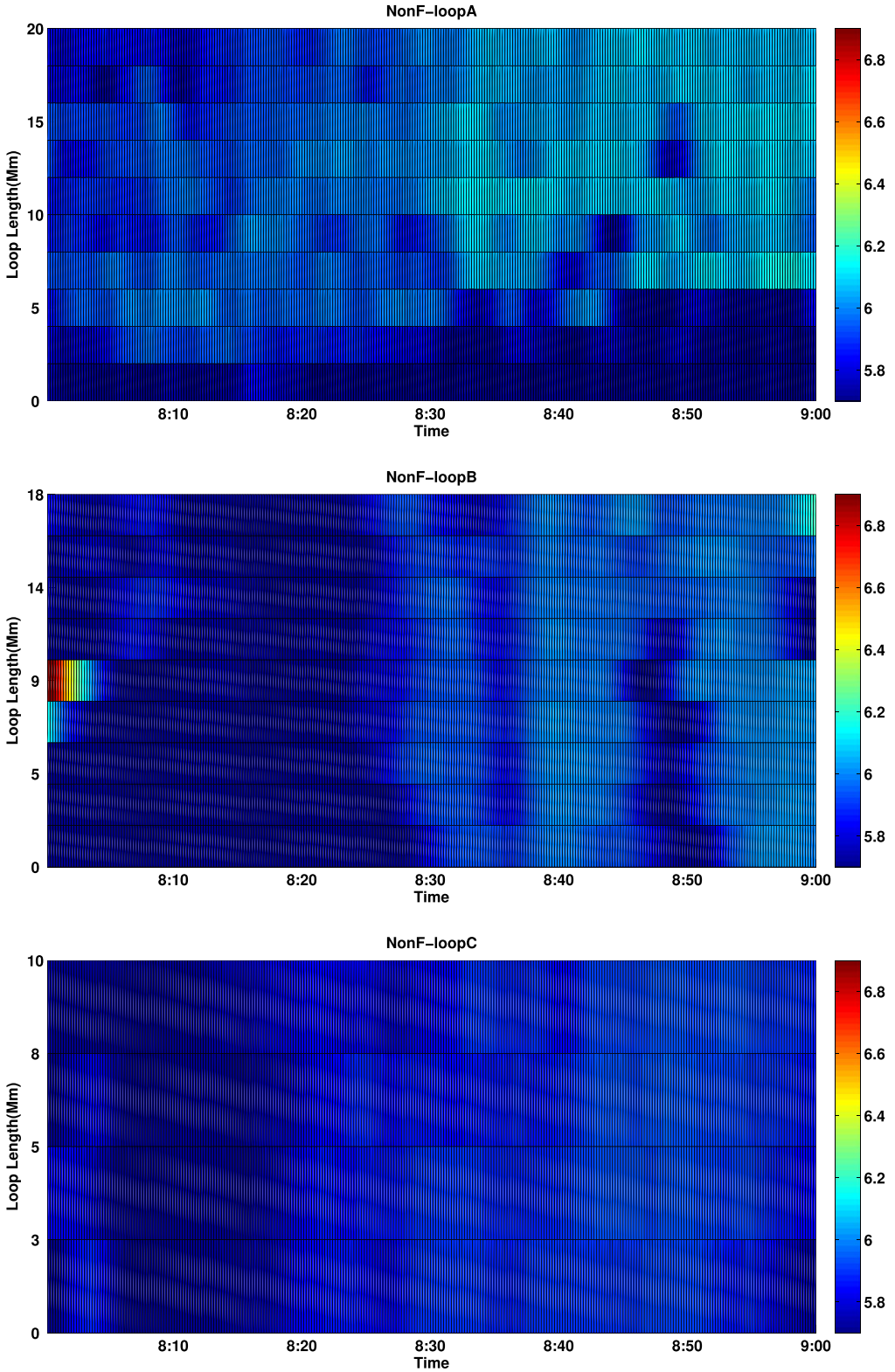

Figure 7. From top to bottom: Temperature map of the nonf Loops A, B and C as a time-series. The vertical axis is distance along the loop in Mm, and the horizontal axis is time. The color-bar in the left displays the colors considered for the temperature range.

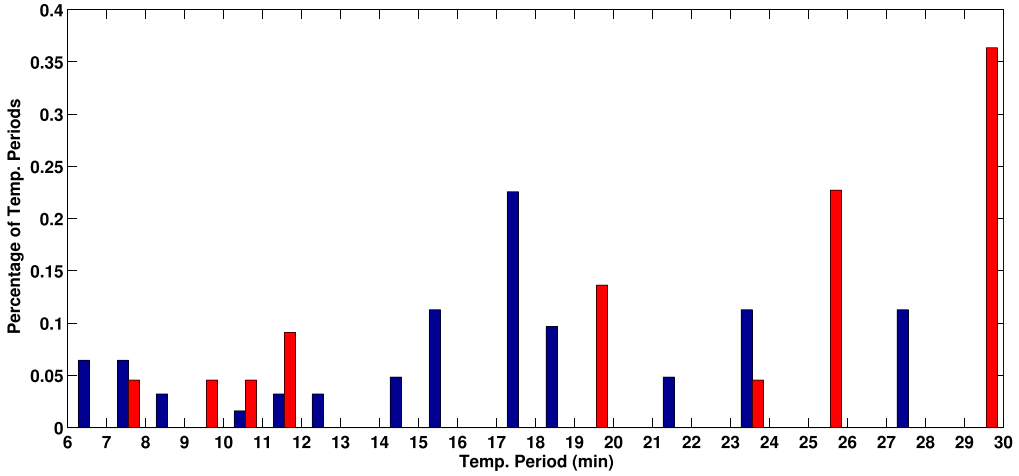

Figure 8. Histogram of the temperature period percentages for the loops' strips of the flaring (blue bars) and nonf (red bars) ARs. The horizontal axis displays the temperature periods in minutes.

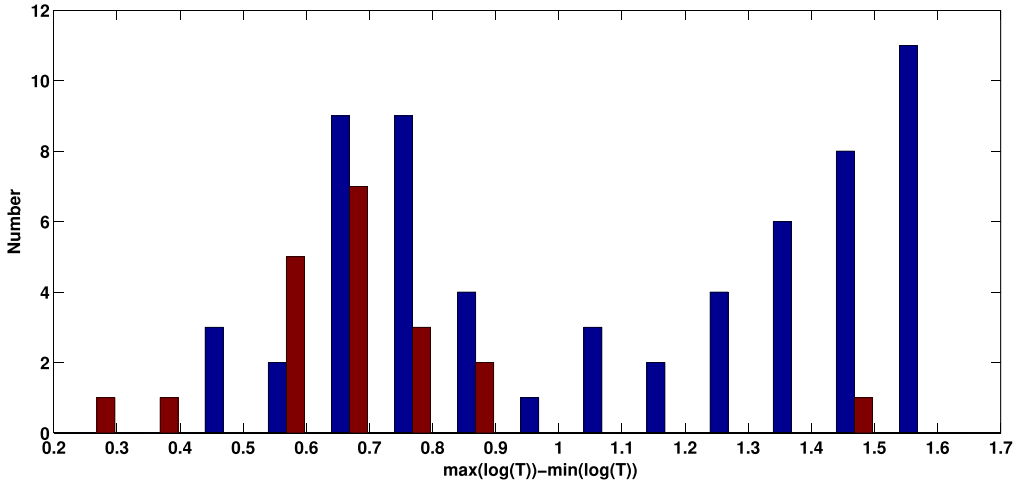

Figure 9. Histogram of the parameter of (max(log(T))–min(log(T))) for each strip of the loops of the flaring (blue bars) and nonf (red bars) ARs.

difference between maximum and minimum of the temperature value (max(log(T))–min(log(T))), are much higher on average for the loops' strips of the flaring AR in comparison with the loops' strips of the nonf one.

5. Summary

We reported the temperature oscillations of coronal loops of a flaring AR. We selected the flaring AR 11283 to investigate the thermal structure and treatment of its loops. This region includes a high energy flare x2.1 and the transverse oscillations of two loops associated with it were analyzed before by Jain et al. (2015). They analyzed intensity variations in the wavelength 171 Å in two coronal loops of this region and detected obvious transverse oscillation with periods of roughly 2 minutes and decay times of 5 minutes for these loops (Loops A and B in Figure 1(b)) at the flare time. We were curious to know if the temperature variations follow the transverse oscillations of the loops, or if there is any relation or correlation between them. We also wanted to investigate the thermal fluctuations at the flare time. As a blind test to see the specific thermal properties of the flaring loops, we selected an LOS nonf AR (12194), extracted three segments of its loops and analyzed their thermal treatment. Then we compared the temperature treatment of the loops at the flaring region with the loops of the nonf region to see the differences. We were eager to observe the probable discrepancies between flaring and nonf loops in this respect.

Here we used data of three loops of the flaring AR (AR 11283) around the time of the Flare X2.1, from 22:10 UT until

23:00 UT on 2011 September 6, plus three loops of the nonf AR (AR 12194), from 08:00:00 UT until 09:00:00 UT of 2014 October 26 (marked in Figures 1 and 2). To calculate the time series of the loop temperature values, we first extracted the loop pixels in each image and then displayed the loop straightly for all the images in the time series of different wavelengths. To do thermal analysis, we used the spatially synthesized Gaussian DEM forward-fitting method proposed by Aschwanden et al. (2015). We calculated the peak temperatures for each strip of the loops. Then we applied the Lomb–Scargle method to analyze temperature oscillations of the time-series for each strip of the loops.

We observed temperature oscillations which are following the transverse loop oscillations observed by Jain et al. (2015) for the flaring loops. Furthermore, the temperature oscillations in these flaring loops happen before the transverse oscillations start and continue even in the time duration after the transverse oscillations decay. As observed, the temperature oscillations do not decay as rapidly as the transverse oscillations do. Conversely, the strips' temperatures increase at the end of the oscillating mode and a rather sensible rise is observed in the final temperatures of the f-loops' segments. The ranges of the obtained periods are from 7 to 28.4 minutes for the flaring loops, and from 8.5 to 30 minutes for the nonf loops. With the onset of an X-flare in F-Loop A, which has a distinct transverse oscillation in the flaring time with period of roughly 2 minutes and decay time of 5 minutes, a temperature oscillation is observed with periods of roughly 10–28.5 minutes in different segments of this loop, and as the transverse oscillation decays in this interval, no special definite decay is observed in its temperature oscillations.

The temperature periods of the flaring loops are rather shorter than the temperature periods of the nonf loops. The loops of the flaring region display some short temperature oscillation periods in which some are less than 10 minutes (Table 1). Such short periods are more frequently observed for the loops of the flaring AR and, in the case of the nonf ones, are very scarce. We observed that the periods of the flaring loops have more diversity than those of the nonf ones. Based on our confined observations, the nonf loops' periods are longer and their temperature values are all lower. So, our research showed that thermal structures of the flaring loops differ from the nonf ones in the ways described above. As temperature maps demonstrate, the temperature fluctuations are increasing at the flaring time and around 20 minutes after, in the flaring loops. This happens with some oscillations in strips' temperature. Conversely, it seems that different strips of the nonf loops have relatively more similar temperature fluctuations. The temperatures are both higher on average in the flaring loops' segments as expected. The significances of the periods, obtained by the Lomb–Scargle method, are calculated for each strip of each loop and the results affirm that these significances for the loops' strips of the flaring region are high and close to one, while for the loops' strips of the nonf region are less than 0.5. Hence the detected periods in the flaring loops' strips have high significances (near to one) and are oscillations, whereas the detected periods in the nonf loops' strips have less significances in comparison with the flaring ones, and maybe they are just fluctuations.

Using this method for the coronal loops showed that the oscillation modes obtained for the temperatures of the flaring loops are very close to those of the spatial slow-mode oscillations of the coronal loops, so the origin of temperature oscillation is probably slow-mode waves. Such kind of oscillations often occur in hot coronal loops ($\log(T) > 6$) of ARs, especially the ones associated with small (or micro) flares (Wang et al. 2021). The loops of our flaring AR are also hot loops with the mean temperature above this range. They also display intensity oscillations. Hence we think the above evidence confirms the slow-mode oscillations for flaring loops. The temperature of the nonf loops is lower ($\log(T) < 6$) and, as discussed above, we believe that the observed oscillation-like periods in nonf loops should be more probably related to the high amplitude fluctuations.

Comparing the loops of the flaring and nonf regions, we observed that the amplitudes of the fluctuations show a discrepancy. The averages of the parameter (Max($\log T$)–Min($\log T$)) in F-Loop A, F-Loop B1, F-Loop B2, F-Loop C1 and F-Loop C2 are 1.21, 1.10, 0.81, 1.48 and 0.88, respectively, and for the nonf region, means of (Max($\log T$)–Min($\log T$)) are 0.81, 0.62 and 0.56, for nonfloops A, B and C respectively. Therefore the values of the quantity averages of (Max($\log T$)–Min($\log T$)) for these nonf loops manifest a difference from the flaring ones and are lower.

Loops of the nonf AR 12194 have a relatively uniform temperature at the beginning of the time interval, which rises slightly at its end. As the Solar Monitor reports in the neighborhood of this region, the flaring AR 12192 happens between multiple flares, and there is a c4.6 class flare occurring at 9:44 UT. Therefore, a possible explanation could be that the abovementioned slight temperature rise in the loops of AR 12194 (in the time interval 8:00–9:00) originated from the influence of an increase in the energy during the pre-flare conditions which exist in AR 12192.

Hence as our study shows, the temperature of coronal loops of flaring AR changes in an oscillatory manner. Compared with these nonf loops, the flaring loops show higher temperatures on average and higher oscillation periods with higher peaks and deeper valleys. More accurate commentary in this respect requires more extensive statistical research and broader observations.

Acknowledgments

The author Narges Fathalian wishes to also express her thanks for the technical support and comments which were

received from Dr. Farhad Daii and Dr. Mohsen Javaherian regarding this work.

References

Abedini, A., Safari, H., & Nasiri, S. 2012, SoPh, 280, 137
Anfinogentov, S., Nakariakov, V. M., Mathioudakis, M., Van Doorsselaere, T., & Kowalski, A. F. 2013, ApJ, 773, 156
Aschwanden, M. J., Boerner, P., Schrijver, C. J., & Malanushenko, A. 2013, SoPh, 283, 5
Aschwanden, M. J. 2006, RSPTA, 364, 417
Aschwanden, M. J., & Boerner, P. 2011, ApJ, 732, 81
Aschwanden, M. J., Boerner, P., Ryan, D., et al. 2015, ApJ, 802, 53
Aschwanden, M. J., Fletcher, L., Schrijver, C. J., & Alexander, D. 1999, ApJ, 520, 880
Ballai, I., Jess, D. B., & Douglas, M. 2011, A&A, 534, A13
Banerjee, D., Erdélyi, R., Oliver, R., & O'Shea, E. 2007, SoPh, 246, 3
Berghmans, D., & Clette, F. 1999, SoPh, 186, 207
Boerner, P., Edwards, C., Lemen, J., et al. 2012, SoPh, 275, 41
Dahlburg, R. B., Einaudi, G., Ugarte-Urra, I., Rappazzo, A. F., & Velli, M. 2018, ApJ, 868, 116
De Moortel, I. 2005, RSPTA, 363, 2743
De Moortel, I., & Brady, C. S. 2007, ApJ, 664, 1210
De Moortel, I., Ireland, J., & Walsh, R. W. 2000, A&A, 355, L23
De Moortel, I., & Nakariakov, V. M. 2012, RSPTA, 370, 3193
Fathalian, N. 2019, arXiv:1908.11369
Fathalian, N., & Safari, H. 2010, ApJ, 724, 411
Fathalian, N., Safari, H., & Nasiri, S. 2010, NewA, 15, 403
Goossens, M., Hollweg, J. V., & Sakurai, T. 1992, SoPh, 138, 233
Gruszecki, M., Murawski, K., Selwa, M., & Ofman, L. 2006, A&A, 460, 887
Guennou, C., Auchère, F., Soubrié, E., et al. 2012a, ApJ, 203, 25
Guennou, C., Auchère, F., Soubrié, E., et al. 2012b, ApJ, 203, 26
Habbal, S. R., & Rosner, R. 1979, ApJ, 234, 1113
Hindman, B. W., & Jain, R. 2014, ApJ, 784, 103
Jain, R., Maurya, R. A., & Hindman, B. W. 2015, ApJL, 804, L19
Jess, D. B., Reznikova, V. E., Ryans, R. S. I., et al. 2016, NatPh, 12, 179
Kolotkov, D. Y., Nakariakov, V. M., & Zavershinskii, D. I. 2019, A&A, 628, A133
Krishna Prasad, S., Jess, D. B., & Van Doorsselaere, T. 2019, FrASS, 6, 57
Li, L. P., Peter, H., Chen, F., & Zhang, J. 2015, A&A, 583, A109
Liu, W., & Ofman, L. 2014, SoPh, 289, 3233
Luna, M., Terradas, J., Oliver, R., & Ballester, J. L. 2010, ApJ, 716, 1371
McClymont, A. N., & Craig, I. J. D. 1985, ApJ, 289, 834
McLaughlin, J. A., Nakariakov, V. M., Dominique, M., Jelínek, P., & Takasao, S. 2018, SSRv, 214, 45
Nakariakov, V. M., Afanasyev, A. N., Kumar, S., & Moon, Y. J. 2017, ApJ, 849, 62
Nakariakov, V. M., Inglis, A. R., Zimovets, I. V., et al. 2010, PPCF, 52, 124009
Nakariakov, V. M., Ofman, L., Deluca, E. E., Roberts, B., & Davila, J. M. 1999, Sci, 285, 862
Nakariakov, V. M., & Verwichte, E. 2005, LRSP, 2, 3
Nisticò, G., Nakariakov, V. M., & Verwichte, E. 2013, A&A, 552, A57
Nisticò, G., Polito, V., Nakariakov, V. M., & Del Zanna, G. 2017, A&A, 600, A37
Ofman, L., & Wang, T. 2002, ApJL, 580, L85
Pant, V., Tiwari, A., Yuan, D., & Banerjee, D. 2017, ApJL, 847, L5
Pascoe, D. J., Nakariakov, V. M., & Arber, T. D. 2007, SoPh, 246, 165
Reale, F., Testa, P., Petralia, A., & Kolotkov, D. Y. 2019, ApJ, 884, 131
Roberts, B., Edwin, P. M., & Benz, A. O. 1984, ApJ, 279, 857
Romano, P., Zuccarello, F., Guglielmino, S. L., et al. 2015, A&A, 582, A55
Russell, A. J. B., Simões, P. J. A., & Fletcher, L. 2015, A&A, 581, A8
Scargle, J. D. 1982, ApJ, 263, 835
Schmelz, J. T., Jenkins, B. S., Worley, B. T., et al. 2011, ApJ, 731, 49
Schmelz, J. T., Kimble, J. A., Jenkins, B. S., et al. 2010, ApJL, 725, L34
Schmelz, J. T., Pathak, S., Brooks, D. H., Christian, G. M., & Dhaliwal, R. S. 2014, ApJ, 795, 171
Schmelz, J. T., Pathak, S., Jenkins, B. S., & Worley, B. T. 2013, ApJ, 764, 53
Ugarte-Urra, I., & Warren, H. P. 2014, ApJ, 783, 12
Van Doorsselaere, T., Kupriyanova, E. G., & Yuan, D. 2016, SoPh, 291, 3143
Van Doorsselaere, T., Wardle, N., Del Zanna, G., et al. 2011, ApJL, 727, L32
VanderPlas, J. T. 2018, ApJ, 236, 16
Verwichte, E., Nakariakov, V. M., Ofman, L., & Deluca, E. E. 2004, SoPh, 223, 77
Wang, T. 2011, SSRv, 158, 397
Wang, T., Innes, D. E., & Qiu, J. 2007, ApJ, 656, 598
Wang, T., & Ofman, L. 2019, ApJ, 886, 2
Wang, T., Ofman, L., Sun, X., Provornikova, E., & Davila, J. M. 2015, ApJL, 811, L13
Wang, T., Ofman, L., Yuan, D., et al. 2021, SSRv, 217, 34
Wang, T. J., & Solanki, S. K. 2004, A&A, 421, L33
Wang, T. J., Solanki, S. K., Innes, D. E., Curdt, W., & Marsch, E. 2003, A&A, 402, L17
Warren, H. P., Winebarger, A. R., & Brooks, D. H. 2012, ApJ, 759, 141
Wills-Davey, M. J., & Thompson, B. J. 1999, SoPh, 190, 467